Chemical Science

ROYAL SOCIETY OF CHEMISTRY

EDGE ARTICLE

View Article Online
View Journal | View Issue

Cite this: *Chem. Sci.*, 2024, **15**, 5152

All publication charges for this article have been paid for by the Royal Society of Chemistry

Oxidation-induced ambiphilicity triggers N–N bond formation and dinitrogen release in octahedral terminal molybdenum(v) nitrido complexes†

C. Christopher Almquist, [a] Thayalan Rajeshkumar,[b] H. D. A. Chathumal Jayaweera,[a] Nicole Removski,[a] Wen Zhou,[a] Benjamin S. Gelfand,[a] Laurent Maron*[b] and Warren E. Piers *[a]

Coupling of octahedral, terminal d^1 molybdenum(v) nitrido complexes supported by a dianionic pentadentate ligand *via* N–N bond formation to give μ-dinitrogen complexes was found to be thermodynamically feasible but faces significant kinetic barriers. However, upon oxidation, a kinetically favored nucleophilic/electrophilic N–N bond forming mechanism was enabled to give monocationic μ-dinitrogen dimers. Computational and experimental evidence for this "oxidation-induced ambiphilic nitrido coupling" mechanism is presented. The factors influencing release of dinitrogen from the resulting μ-dinitrogen dimers were also probed and it was found that further oxidation to a dicationic species is required to induce (very rapid) loss of dinitrogen. The mechanistic path discovered for N–N bond formation and dinitrogen release follows an ECECC sequence (E = "electrochemical step"; C = "chemical step"). Experimental evidence for the intermediacy of a highly electrophilic, cationic d^0 molybdenum(vi) nitrido in the N–N bond forming mechanism *via* trapping with an isonitrile reagent is also discussed. Together these results are relevant to the development of molecular catalysts capable of mediating ammonia oxidation to dihydrogen and dinitrogen.

Received 4th January 2024
Accepted 16th February 2024

DOI: 10.1039/d4sc00090k

rsc.li/chemical-science

Introduction

Oxidation of ammonia (NH_3) to dihydrogen (H_2) and dinitrogen (N_2) offers a vector for production of green hydrogen if the energy required to drive the reaction (and the manufacture of NH_3) can be obtained from renewable energy sources.[1] Catalysts are required for selective reactions and molecular transition metal complexes for the oxidation of NH_3 to N_2 and H_2 (ref. 2) have seen renewed interest in the last few years.[1,3–7] This was spurred in part upon recognition that many of the compounds that can effectively mediate water oxidation might be applied to ammonia oxidation[8]—without the itinerant hazards of generating O_2/H_2 mixtures. Although not as available as water, ammonia is an abundant feedstock manufactured on a large scale using the Haber–Bosch process *via* the catalytic reduction of N_2 with H_2.[9] Furthermore, ammonia is easier to oxidize than water and is similarly "carbon free" in terms of the end products of oxidation.

Essential steps in the conversion of NH_3 to H_2 and N_2 are the cleavage of three strong N–H bonds, and the formation of an N–N bond.[8] Considered superficially, this seems relatively simple, but there are a variety of mechanisms available for each step when using molecular catalysts. For N–H bond cleavage, coordination-induced bond weakening[10] of the N–H bond(s) of NH_3 upon ligation to a metal can be substantial and the factors that influence the extent to which bond weakening occurs are a subject of current study.[5,11–15] When weakened below a threshold of about 52 kcal mol^{-1}, elimination of H_2 (BDFE = 104 kcal mol^{-1}) becomes thermodynamically feasible and kinetic pathways involving metal hydrides[11] or bimolecular H_2 elimination in coordinatively saturated systems[15] can lead to "spontaneous" loss of H_2 from any of the M–NH_n (n = 3, 2, or 1) intermediates formed *via* loss of hydrogen atoms. Alternatively, use of hydrogen atom abstracting reagents like the 2,4,6-tri-*tert*-butylphenoxy radical (ArO$^\bullet$) can be employed if bond weakening of N–H to values below the strength of the ArO–H bond (74.8 kcal mol^{-1} (ref. 16 and 17)) are achieved.

The other key step, N–N bond formation, can occur from any of these intermediates through nucleophilic attack by external

[a]*Department of Chemistry, University of Calgary, 2500 University Drive NW, Calgary, Alberta, T2N 1N4, Canada. E-mail: wpiers@ucalgary.ca*

[b]*LPCNO, Université de Toulouse, INSA, UPS, Toulouse, France*

† Electronic supplementary information (ESI) available: Experimental and characterization details for all new compounds, including spectroscopic data, X-ray crystallographic data and computational details with the cartesian coordinates for calculated structures (PDF). CCDC 2303932–2303944. For ESI and crystallographic data in CIF or other electronic format see DOI: https://doi.org/10.1039/d4sc00090k

NH_3 (ref. 3, 6, 7, 18 and 19) on (usually cationic) M–NH_n ($n = 2$, 1, 0) intermediates or *via* bimolecular coupling of metal amido[20,21] (to bridging hydrazine), imido[22] (to μ-diazene) or nitrido (to μ-dinitrogen) complexes.[8,14] Nitrogen–nitrogen bond formation *via* coupling of two terminal nitrido complexes is generally thought to take place *via* two limiting paths that depend on the electron distribution in the metal nitrido bond, as shown in Scheme 1.[8] When the nitrido has significant spin density associated with the terminal nitrogen, such that it behaves as a nitridyl radical, bimolecular homocoupling between these two radicals is possible.[4,23–25] Alternatively, in ambiphilic nitrido complexes with energetically matched HOMO nitrido lone pairs and LUMO MN π* orbitals, a nucleophilic/electrophilic N–N coupling mechanism can occur.[26] More commonly, this latter mechanism is observed in nitrido pairs where the metal ligand combinations are different, rendering one L_nMN nucleophilic and the other electrophilic.[27] Between these two limiting extremes there lies a continuum and there is some indication that N–N bond formation between nitridos that utilize both radical character and ambiphilicity make for facile N–N bond formation.[28] It is clear that understanding the factors which control the barrier of N–N bond formation is crucial for developing more effective catalysts, since upon coupling the driving force for N_2 formation and release can be substantial.

We recently reported[15] the synthesis of a neutral Mo(v) nitrido complex supported by a pentadentate diborate ligand (B_2Pz_4Py) related to the neutral pentapyridyl "PY5" framework first prepared by the Feringa[29] and Stack[30,31] groups in the mid 1990's and popularized by Chang and Long as a platform for electrocatalytic applications.[32–35] By virtue of its dianionic L_3X_2 nature, the B_2Pz_4Py ligand[36] lowers the overall charge of its complexes and can stabilize higher oxidation state complexes in metals from across the d block.[37–43] The complex (B_2Pz_4Py)Mo(v)N, **1-Tol**, was prepared as the end product of removal of three hydrogen atoms from the Mo(ii) neutra ammine complex in the context of probing the coordination-induced bond weakening in these complexes.[15] Here we probe the reactivity and properties of the Mo(v) nitrido complexes of two variants of this dianionic pentadentate system in the context of N–N bond formation and provide evidence for a distinct oxidation-induced nucleophilic/electrophilic coupling pathway for N–N bond formation.

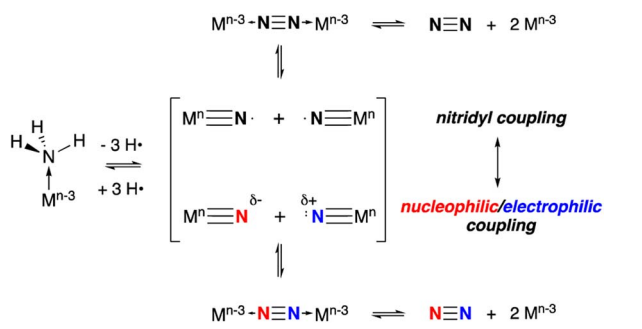

Scheme 1 Limiting mechanisms of N–N bond formation *via* coupling of two terminal metal nitrido complexes.

Results and discussion

In our previous report,[15] we showed that the neutral, d^1 molybdenum(v) terminal nitrido complex **1-Tol** could be prepared *via* deprotonation of the cationic imido complex $[(B_2Pz_4Py)Mo(v){=}NH]^+[NTf_2]^-$. However, a one-pot route involving sequential deprotonation of the cationic Mo(iii) ammine complex $[(B_2Pz_4Py)Mo(iii)–NH_3]^+[NTf_2]^-$ followed by two hydrogen atom transfers using the ArO$^\bullet$ reagent mentioned above proved a more convenient protocol, particularly for preparing the ^{15}N-labeled nitrido isotopologues (Scheme 2). The nitrido **1-Tol** was fully characterized, including *via* X-ray crystallography.[15] The Mo–$N_{nitrido}$ bond length of 1.729(3) Å was noted to be longer than that observed for the analogous bond length of 1.695(3) Å in the cationic imido precursor and furthermore, the DFT (B3PW91) computed Mo–$N_{nitrido}$ distance in **1-Tol** is 1.660 Å, more in line with expectations. The bonding analysis carried out at the Natural Bonding Orbital (NBO) level indicates as expected the presence of a Mo–N triple bond where the three bonds are highly covalent (see ESI†). In initial studies of the reactivity of **1-Tol**, we noted its very poor solubility in most common solvents and found it to be sparingly soluble only in dichloromethane, chloroform or *N*,*N*-dimethylformamide (DMF). This hampered reactivity studies, particularly for experiments requiring low temperatures (see below). Examination of the crystal packing diagram of **1-Tol** showed an extended ribbon of molecules supported by close contacts (2.576 Å) between the nitrido nitrogen and the *meta*-aryl protons of the tolyl groups incorporated on the ligand borate moieties (Fig. 1a). We hypothesized that these interactions are likely responsible for the poor solubility of nitrido derivative **1-Tol**.

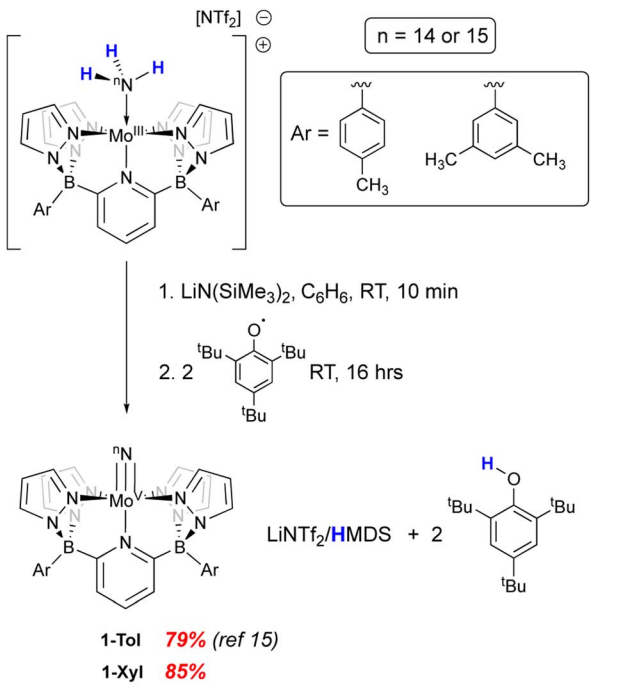

Scheme 2 Synthesis of neutral Mo(v) nitrido derivatives **1-Ar** (Ar = *para*-tolyl, *meta*-xylyl).

The synthetic scheme for preparing the dianionic pentadentate B_2Pz_4Py ligand system[36] is such that modification of the aryl groups on the borates is relatively easy. We postulated that switching from tolyl groups to 3,5-dimethylphenyl substituents would disrupt the intermolecular packing interactions of Fig. 1a and result in a more soluble Mo(v) nitrido derivative. Accordingly, the xylyl-substituted ligand was prepared and used to synthesize the cationic Mo(III) ammine precursor to nitrido **1-Xyl** using previously established protocols[15] (see Scheme S2 and the ESI† for full synthetic and characterization details of complexes incorporating the xylyl-substituted ligand). Compound **1-Xyl** was then prepared in 85% yield as depicted in Scheme 2 and was found to be significantly more soluble in a variety of solvents in comparison to **1-Tol**. Like **1-Tol**, nitrido **1-Xyl** is a d^1 ($\mu_{eff} = 1.71$, by the Evans method[44]) species that is largely NMR silent, although the xylyl methyl groups are assignable in the ^{1}H NMR spectra. X-ray quality crystals were obtained by slow evaporation of solvent from a saturated toluene solution, and the molecular and packing structures are shown in Fig. 1b and c, respectively. In contrast to **1-Tol**, the shortest intermolecular interactions in **1-Xyl** involve the nitrido nitrogen and C–H bonds on an adjacent molecule's pyrazolyl ring and are substantially longer (2.930 and 3.111 Å) than the interactions in **1-Tol**. A shorter Mo–$N_{nitrido}$ distance of 1.674(2) is observed in **1-Xyl**, which is more consistent with the computed value for this bond in the gas phase. Both compounds exhibit Mo–$N_{nitrido}$ stretching frequencies of 1001 cm^{-1} in the solid state IR spectrum (which shifts to 982 cm^{-1} in the $Mo^{15}N_{nitrido}$ isotopologues, see ESI†), suggesting essentially identical bond orders and strengths in these two derivatives.

The d^1 Mo(v) nitridos **1-Ar** exhibit EPR spectra that indicate the unpaired spin is largely metal-based (see Fig. 2 and S1†), with essentially identical g values of 1.966 and a six-line hyperfine coupling pattern ($A = 53$ G) to the ≈25% abundant spin 5/2 $^{95/97}$Mo nuclei. These parameters are typical for d^1 Mo(v) compounds.[45–48] DFT analysis also indicates there is very little spin density associated with the nitrido nitrogen (16%) with most of it residing in a metal-based d-orbital. The SOMO-1 orbital is Mo–$N_{nitrido}$ σ-bonding in character and is essentially the nucleophilic nitrido lone pair, accounting for the moderate nucleophilic character of these neutral Mo(v) nitrido complexes.

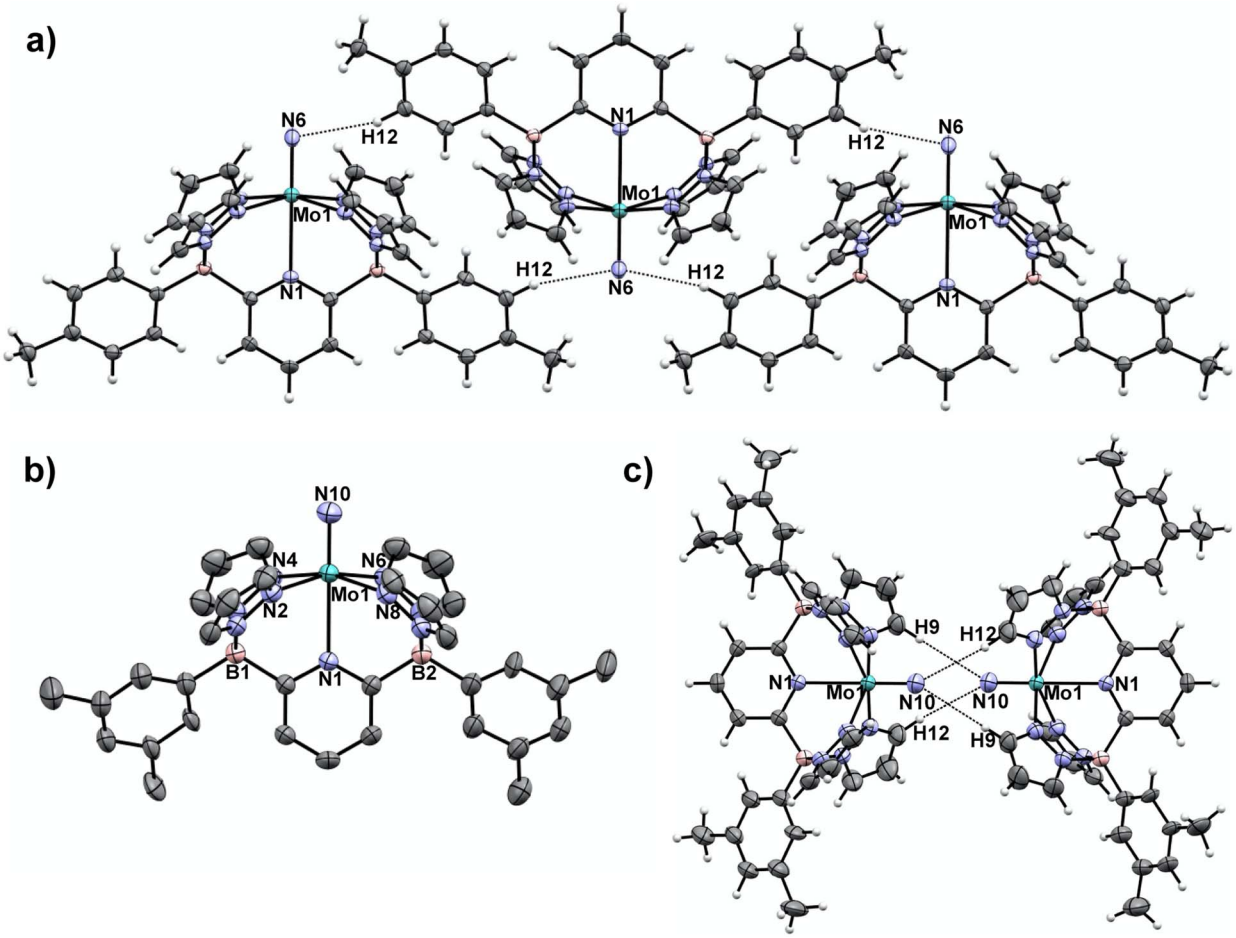

Fig. 1 a) Crystal packing motif for nitrido **1-Tol**[15] with closest intermolecular contacts. Selected intermolecular contact distance (Å): N(6)–H(12), 2.576. (b) Molecular structure of **1-Xyl** Selected bond distances (Å): Mo(1)–N(1), 2.4564(14); Mo(1)–N(10), 1.6740(18). (c) Crystal packing motif for nitrido **1-Xyl** with closest intermolecular contacts. Selected intermolecular contact distance (Å): N(10)–H(9), 2.930; N(10)–H(12), 3.111. Thermal ellipsoids are shown at the 50% probability level and all H atoms except those involved in intermolecular contacts are omitted for clarity.

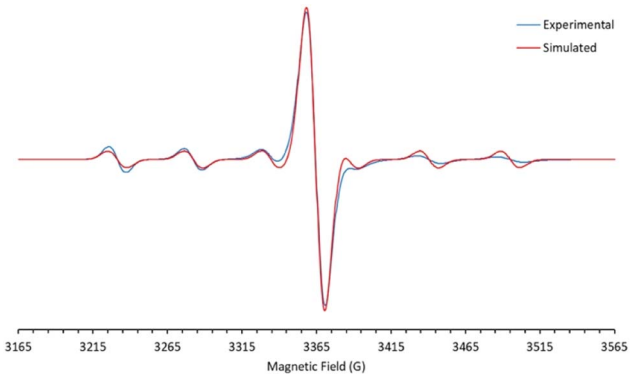

Fig. 2 X-band EPR spectrum of **1-Xyl** in dry toluene (970 μM), taken at 293 K. The experiment was run with a centre field of 3360.0 G and a sweep width of 500.0 G. The time constant and conversion time were set to 2.56 ms and 8.00 ms, respectively. 16 scans were collected. Frequency: 9.258916 GHz. The simulated spectrum was generated in EasySpin, indicating a Mo-based radical with a central line ($I_{Mo} = 0$) $g = 1.966$ with a six-line spectrum ($I_{Mo} = 5/2$) $A_{Mo} = 52.82$ G.

Given these characteristics, it is perhaps unsurprising that these terminal nitridos exhibit substantial thermal stability towards N–N bond formation *via* bimolecular coupling. For **1-Tol**, solutions heated at 50 °C in $CDCl_3$ gradually (over the course of 12 weeks) undergo conversion to the previously reported chlorido complex[15] [(B_2Pz_4Py)Mo(III)–Cl]. No intermediates were observed and although N_2 is presumed to be eliminated, it was not directly detected in this experiment, which was conducted on a rather small scale. Solutions of **1-Xyl** in toluene at 100 °C undergo similarly slow conversion to a new product identified separately (see below) as the neutral μ-dinitrogen dimer **3-Xyl** along with traces of the μ-nitrido complex **2-Xyl**, which is the xylyl analog of the previously reported dinuclear μ-nitrido complex **2-Tol**;[15] the spectral characteristics of **2-Xyl** were confirmed by its separate synthesis and characterization (see ESI† for details). As shown in Scheme 3, we hypothesize that slow, rate-determining bimolecular coupling occurs to give the bridging dinitrogen dimers **3-Ar**, which we assign as having Mo(III)–N=N–Mo(III) rather than Mo(II)–N≡N–Mo(II) character based on the observed ^{11}B NMR chemical shift of −153.5 ppm‡ for **3-Xyl** and computational interrogation of this species (see below). In addition to this evidence for **3-Xyl**, the $^{15}N_2$ isotopologue was confirmed to be produced by mass spectrometry (Fig. S2†). In the case of coupling from **1-Tol** in $CDCl_3$ at 50 °C, **3-Tol** is not observed but is oxidized to the [($^{Tol}B_2Pz_4Py$)Mo(III)–Cl] product by the solvent. We presume that in the coupling of **1-Xyl**, the harsh conditions of the experiment can lead to reaction of **3-Xyl** with **1-Xyl** to give the traces of μ-nitrido complex we observe spectroscopically, but this is a very slow process even relative to the slow N–N bond formation observed for coupling of **1-Xyl**. The bottom line is that, in both complexes, conversion of compounds **1-Ar** to dimers **3-Ar** *via* nitrido–nitrido coupling is extremely slow under the conditions employed.

Since N–N bond formation from these d^1 Mo(V) nitridos is so inefficient, we probed their redox properties by cyclic voltammetry. Both complexes **1-Ar** are oxidized irreversibly at moderate potentials ($E_{ox} = 0.62$ V *vs.* Fc/Fc^+ for **1-Xyl** and 0.57 V for **1-Tol**) and the observed irreversibility is maintained at all scan rates employed (25–1600 mV s^{-1}, see Fig. S3†). This is suggestive of a facile chemical reaction triggered by oxidation and to probe the nature of this reactivity, chemical oxidation using a family of brominated triarylammoniumyl radical cations $[N(Ar)_3]^{\bullet+}$, partnered with Krossing's perfluorinated tetra-*tert*-butoxy aluminate weakly coordinating anion[49] was undertaken. Here, we have utilized "Magic Blue" (**MB**$^{\bullet+}$, Ar = 4-BrC_6H_4; $E^\circ = +0.70$ V *vs.* Fc/Fc^+ in DCM[50]), and Magic "Blue's Cousin"[51] (**BC**$^{\bullet+}$, Ar = 2-Br-4-*tert*-butyl-C_6H_3, $E^\circ = +0.78$ V *vs.* Fc/Fc^+ in DCM), the latter being a more soluble derivative for use at lower temperatures. The Krossing anion was used because other WCAs[52] were either chemically non-innocent (*e.g.* $[SbX_6]^-$, X = F or Cl) or not well-behaved from a solubility or physical perspective (*e.g.*, $[NTf_2]^-$ or $[B(C_6F_5)_4]^-$). Krossing's aluminate anion proved both chemically inert and useful in promoting crystallizable products.

Initial experiments involving oxidation of **1-Tol** with one equivalent of **MB**$^{\bullet+}$ at room temperature produced a mixture of products but the reactions proceeded much more cleanly when only 0.5 equivalents of oxidant were employed. As shown in Fig. 3, treatment of either nitrido **1-Ar** with 0.5 equivalents of **MB**$^{\bullet+}$ result in a rapid elimination of N_2 and production of the cationic μ-nitrido dinuclear compounds **[2-Ar]**$^+$ as the major products (≈95% NMR yields). Although not quantified, the eliminated N_2 was confirmed as originating from the nitrido nitrogens by detecting $^{15}N_2$ *via* NMR spectroscopy (≈ −69 ppm (ref. 14 and 53)) and GCMS (Fig. S4†). The cationic dinuclear products were fully characterized by preparing them separately *via* oxidation of the neutral **2-Ar** μ-nitridos, NMR spectroscopy, and X-ray crystallography (Fig. 3). The Mo(1)–N(10)–Mo(2) angle is essentially linear (176.52(19)°) and Evans method measurement of the μ_{eff} indicates an $S = 2$ ground state and therefore a formally Mo(IV)=N=Mo(IV) configuration where electronic coupling across the nitrido bridge is minimal. In comparison, the Mo–N(10) bonds in **[2-Ar]**$^+$ relative to the analogous bonds in the neutral precursors undergo minimal change. Oxidatively-induced N_2 elimination[54–56] from terminal nitrido complexes has been observed in the well-studied d^2 Mn(V)N complexes supported by tetradentate Schiff base type ligands.[57] In these systems, oxidation to a d^1 cationic $[Mn(VI)N]^+$ imbues significant nitridyl character to these species and Storr *et al.* in particular convincingly demonstrated that bimolecular coupling of these nitridyls (Scheme 1) was the likely mechanism of N–N bond formation for that family of compounds.[54] In the present molybdenum system, oxidation of d^1 nitridos **1-Ar** presumably leads to a d^0 $[Mo(VI)N]^+$; bimolecular coupling of this species is unlikely on both electrostatic and orbital grounds. Indeed, DFT analysis of the barriers to N–N bond formation from homocoupling of either **1-Tol** or **[1-Tol]**$^+$, show that these reactions, while exergonic, have prohibitively high barriers of 33 and 54 kcal mol^{-1} at room temperature, respectively (Fig. 4). The former value is certainly consistent with the experimentally observed slow loss of $^nN_2$ from compounds **1-Ar**, Scheme 3, but the significantly higher barrier to N–N bond formation from **[1-**

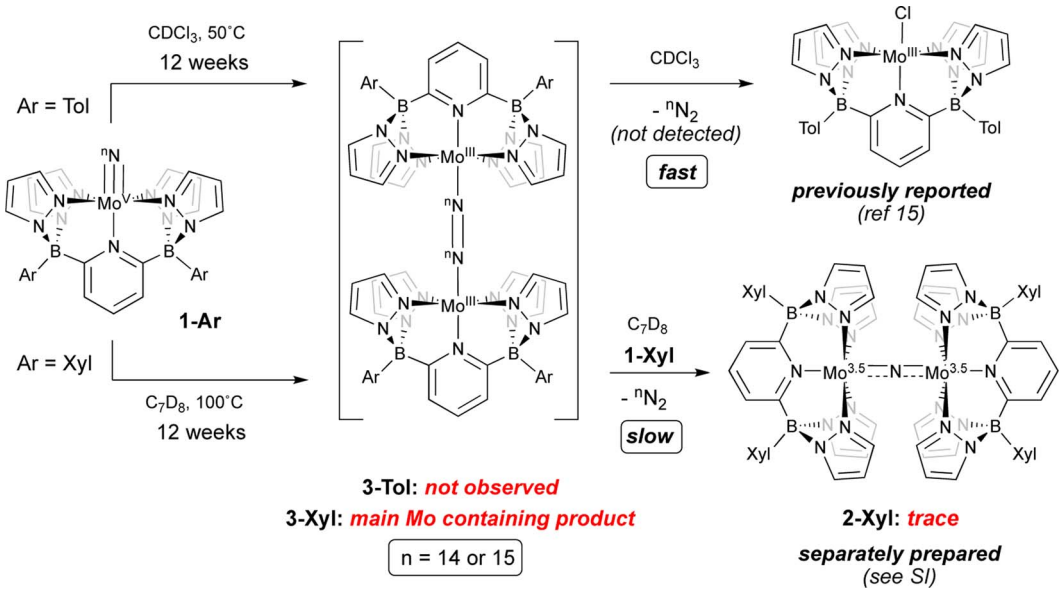

Scheme 3 Thermally induced coupling of terminal neutral Mo(v) nitrido complexes **1-Ar**.

Ar]$^+$ initially seemed at odds with the very rapid loss of N_2 upon generation of these cations. However, as revealed in Fig. 4, the barrier to heterocoupling of neutral (nucleophilic) nitride **1-Tol** with cationic (electrophilic) nitride **[1-Tol]**$^+$ is much lower at 16 kcal mol^{-1}, strongly suggesting a nucleophilic/electrophilic mechanism for this oxidation induced N–N bond forming reaction as shown in Scheme 4. As shown in the upper right of Fig. 4, the TS adopts a typical "zig-zag" geometry,[27,58] and the

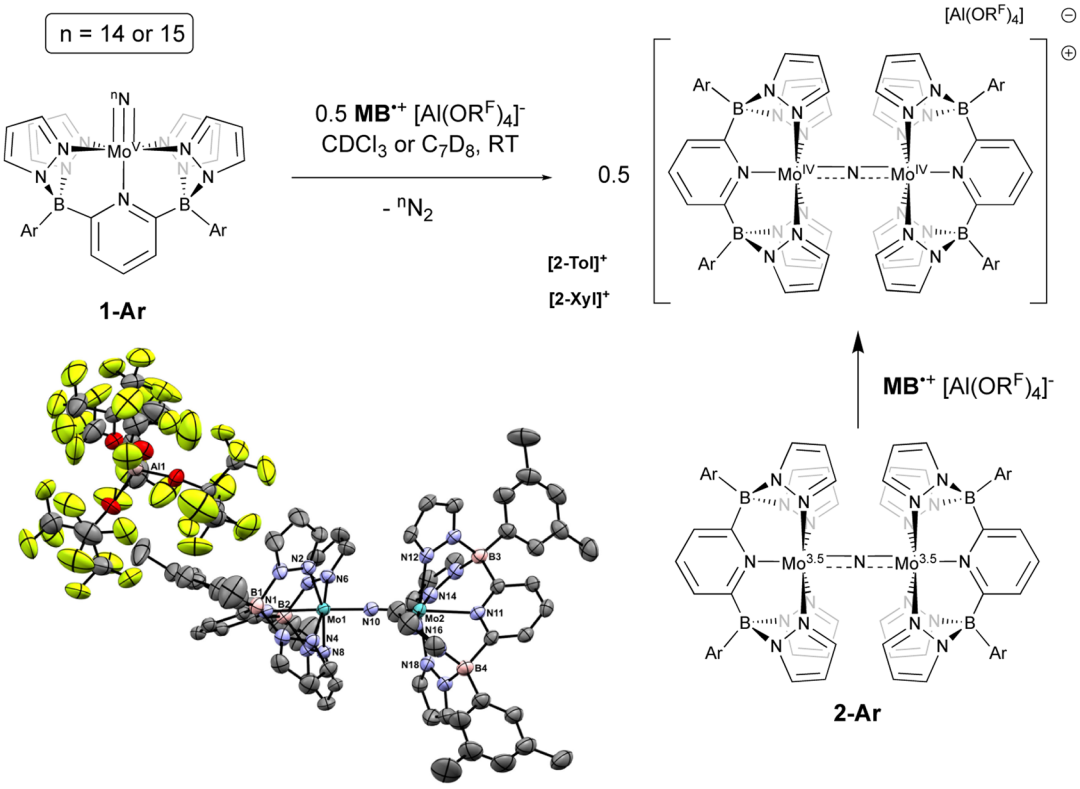

Fig. 3 Oxidation of neutral nitrido **1-Ar** with 0.5 equivalents of **[MB•]**$^+$[Al(OR^F)$_4$]. Lower left: molecular structure of **[2-Xyl]**$^+$[Al(OR^F)$_4$]. Thermal ellipsoids are shown at the 50% probability level and all H atoms are omitted for clarity. Selected bond distances (Å): Mo(1)–N(10), 1.856(3); Mo(2)–N(10), 1.859(3); Mo(1)–N(1), 2.260(3); Mo(2)–N(11), 2.265(3). Selected bond angles (°): Mo(1)–N(10)–Mo(2), 176.52(19).

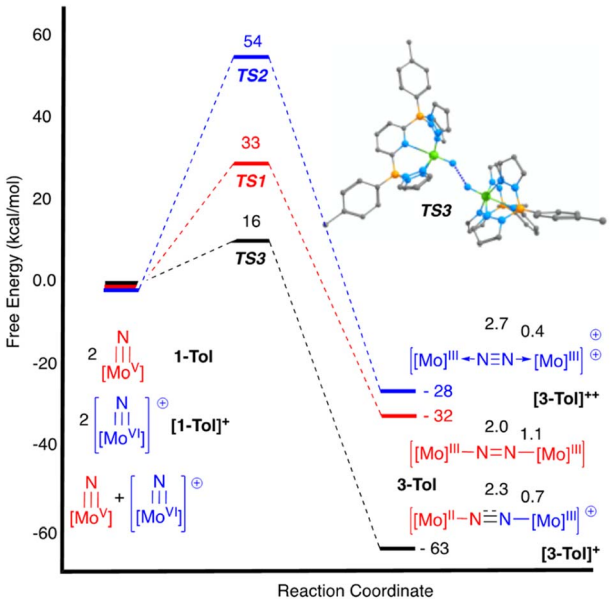

Fig. 4 DFT (B3PW91) computed enthalpy profiles for N–N bond formation *via* bimolecular coupling of **1-Tol** (all red), **[1-Tol]**$^+$ (all blue) and **1-Tol**/**[1-Tol]**$^+$ (mixed red/blue) at room temperature. The energies are given in kcal mol^{-1} and computed Wiberg Bond Index values for the N–N and Mo–N bonds in the μ-dinitrogen products of coupling are also shown. Upper right: ball and stick depiction of the transition state for ambiphilic coupling of **1-Tol** and **[1-Tol]**$^+$.

long N–N separation of 2.277 Å is consistent with an early transition state as befits a low barrier/exothermic reaction profile. Oxidation of **1-Ar** removes a mainly d-orbital-based electron and increases the nitrido nitrogen electrophilicity,[59–61] such that nucleophilic attack by remaining **1-Ar** is now kinetically facile. In support of this, Natural Population Analysis[62] (NPA, Tables S19 and S20†) of the natural charges on the Mo and $N_{nitrido}$ atoms of **1-Tol** (Mo = 1.09, N = −0.37) and **[1-Tol]**$^+$ (1.24, −0.24) show significantly more positive values for the oxidized species indicating a much more electrophilic species. We believe this "induced ambiphilicity" is a distinct

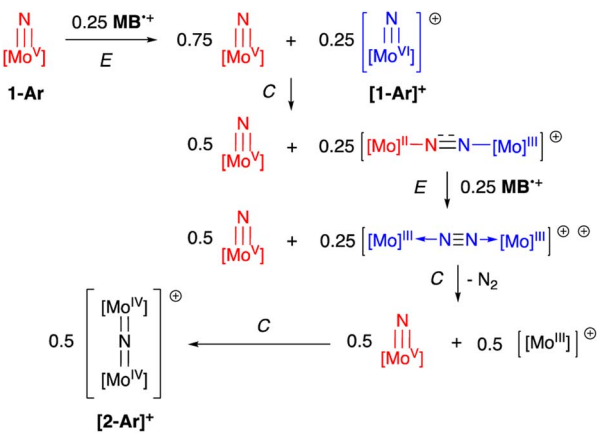

Scheme 4 Oxidation-induced nucleophilic/electrophilic N–N bond formation in Mo(v) nitrides: ECECC mechanism.

mechanistic pathway for N–N bond formation from a single metal nitrido species and contrasts with a path where the nitrido is fully oxidized and undergoes coupling of two nitridyls as in the MnSalen system mentioned above.[54]

The fact that only 0.5 equivalents of oxidant is needed for this reaction is not in itself conclusive evidence for the mechanistic proposal in Scheme 4, since the same products and product distribution would result from homocoupling of the cationic nitridos **[1-Ar]**$^+$ (see Scheme S1†). The DFT results of Fig. 4 also do not directly address the question of which μ-dinitrogen complex most efficiently releases N_2, since the energies depicted do not reflect the relative thermodynamic stabilities of the μ-dinitrogen products, nor the barriers to N_2 release. Having said that, the WBI values (Table S6†) for the N–N and Mo–N bonds calculated certainly suggest release of N_2 from dication **[3-Ar]**$^{++}$ should be most favored as this species has a nearly fully formed nitrogen–nitrogen triple bond.[63,64] Thus the DFT results are highly suggestive that the ambiphilic coupling is kinetically favored, but that N_2 release from the resulting monocationic μ-dinitrogen complex **[3-Ar]**$^+$ is not necessarily thermodynamically feasible. Therefore, we sought experimental evidence for the oxidation-induced nucleophilic/electrophile N–N coupling mechanism of Scheme 4 by conducting the oxidations of **1-Ar** at low temperature and monitoring spectroscopically. At this juncture, the purpose for preparing the more soluble **1-Xyl** derivative becomes apparent; **1-Tol** could not be employed in these experiments due to extremely low solubility in all solvents below 0 °C. However, **1-Xyl** readily dissolves in toluene at −78 °C, and use of the more soluble **BC**$^{\bullet+}$ oxidant allowed us to monitor this process effectively by ^{1}H NMR spectroscopy.

Mixing **1-Xyl** with 0.5 equivalents of **[BC**$^\bullet$**]**$^+$**[Al(OR**^{F}**)**$_4$**]**$^-$ in toluene at −78 °C leads to a homogeneous solution and no apparent reaction between the reagents (Fig. S5†). The sample was warmed in ≈5 °C increments and as it approached −60 °C, evidence of electron transfer was observed as signals for the triarylamine produced upon reduction of **BC**$^{\bullet+}$ emerged in the diamagnetic region of the spectrum. As further warming took place, at about −40 °C signals for two paramagnetic molybdenum products began to grow in until at room temperature these were present in an approximately 1 : 1 ratio. The set of broad signals for one of these products matched those found for **[2-Xyl]**$^+$, while the second, much sharper, set of signals belong to a new, previously unobserved product.

Crystals deposited from these experiments proved to be of X-ray quality and their analysis showed them to be mixtures of μ-nitrido cation **[2-Xyl]**$^+$ and the cationic μ-dinitrogen dimer **[3-Xyl]**$^+$ (Scheme 5 and Fig. 5), which is the new product that arises from the ambiphilic coupling of **1-Xyl** and **[1-Xyl]**$^+$. The structure of this cationic dinitrogen dimer is depicted in Fig. 5 and shows a moderately activated N–N bond elongated to 1.162(7) Å by the lower valent molybdenum centers. That it is isolable and relatively stable towards loss of N_2 is supported by the computed kinetic and thermodynamic properties of N_2 release from **[3-Xyl]**$^+$, which is endothermic by 20 kcal mol^{-1} and has a barrier of 30 kcal mol^{-1} (Scheme S4†). In stark contrast, loss of N_2 from the dicationic **[3-Xyl]**$^{2+}$ is computed to be kinetically facile

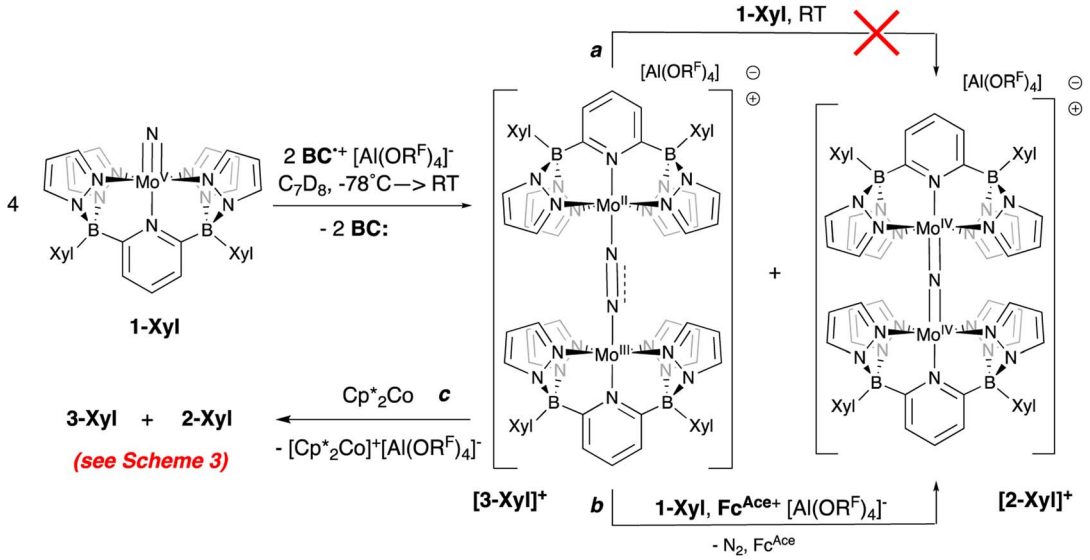

Scheme 5 Reaction of **1-Xyl** with 0.5 equivalents of oxidant at −78 °C and subsequent transformations of the 1 : 1 mixture of [**3-Xyl**]$^+$: [**2-Xyl**]$^+$.

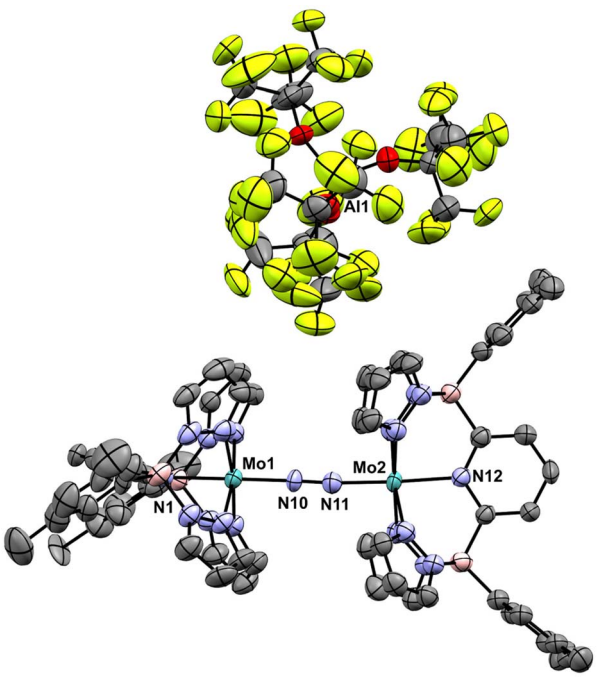

Fig. 5 Molecular structure of [**3-Xyl**]$^+$. Thermal ellipsoids are shown at the 50% probability level and all H atoms are omitted for clarity. Selected bond distances (Å): Mo(1)–N(1), 2.167(5); Mo(1)–N(10), 1.885(5); Mo(2)–N(12), 2.080(5); Mo(2)–N(11), 1.916(6); N(10)–N(11), 1.162(7) *cf.* N–N distance in free N_2 of 1.098. Selected bond angles (°): N(1)–Mo(1)–N(10), 176.6(2); Mo(1)–N(10)–N(11), 173.8(5); N(10)–N(11)–Mo(2), 175.5(4); N(11)–Mo(2)–N(12), 177.2(3).

(barrier of 6 kcal mol^{-1}) and exothermic (by −26 kcal mol^{-1}) as depicted in Scheme S5.† Experimentally consistent with this DFT analysis, simply adding further amounts of **1-Xyl** to the 1 : 1 product mixture does not immediately lead to N_2 release and conversion to [**2-Xyl**]$^+$ (Scheme 5, top arrow, path a). Prolonged heating of this mixture does lead to some conversion (Fig. S38–S46†). However, if more oxidant is added along with the extra **1-Xyl**, rapid, clean conversion to [**2-Xyl**]$^+$ is observed with release of N_2 (Scheme 5, bottom arrow, path b, Fig. S48–S54†) presumably from [**3-Xyl**]$^{2+}$. Note in this experiment, instead of employing **MB**$^{\bullet+}$, we utilize the acetyl-ferrocenium oxidizing agent (E°_{ox} = 0.27 V (ref. 50) *vs.* Fc/Fc$^+$) partnered with Krossing's anion (see ESI† for the full characterization of this reagent), to match with the E°_{ox} of 0.22 V estimated for the [**3-Xyl**]$^+$/[**3-Xyl**]$^{++}$ couple by cyclic voltammetry (Fig. S37†), while not being strong enough to oxidize either **1-Xyl** (0.62 V) or [**2-Xyl**]$^+$ (0.98 V). Together, these experiments provide strong evidence that N_2 release comes *via* [**3-Xyl**]$^{++}$ and confirms the "ECECC" sequence shown in the proposed mechanism of Scheme 4. In more general terms, the observation and isolation of the mono-cationic μ-dinitrogen intermediate [**3-Xyl**]$^+$ in the low temperature oxidation of **1-Xyl** is convincing experimental evidence that oxidatively-induced N–N bond formation occurs selectively *via* heterocoupling between the nucleophilic **1-Xyl** and electrophilic [**1-Xyl**]$^+$. As a final note regarding Scheme 4, when the 1 : 1 mixture of [**3-Xyl**]$^+$ and [**2-Xyl**]$^+$ is reduced by Cp^*_2Co, the products are a 1 : 1 mixture of the neutral dinuclear species **3-Xyl** and **2-Xyl** (Fig. S57–S60†). Indeed, it was this experiment that helped to identify the former as the major product in the thermally-induced coupling of **1-Xyl** depicted in Scheme 3, since the signals in the ^{1}H NMR spectra for these two experiments indicate the presence of both neutral μ-dinitrogen and μ-nitrido dinuclear compounds. Attempts to separately synthesize pure samples of **3-Xyl** have so far failed, but these studies are ongoing.

Although the (evidently) highly reactive d^0 nitrido cation [**1-Xyl**]$^+$ is strongly implicated in the above chemistry, so far direct evidence for it remains elusive. Low temperature oxidation of **1-Ar** (−78 °C, $CDCl_3$ or CD_2Cl_2) with one equivalent of [**MB**$^\bullet$]$^+$[Al(OR^F)$_4$]$^-$ gave mixed results. Although no diamagnetic

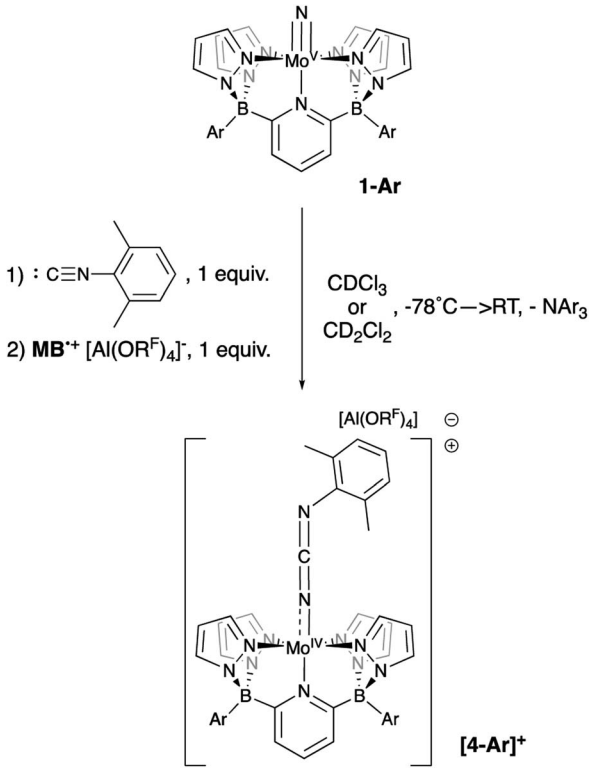

Scheme 6 Reaction of **1-Ar** with 1 equivalent of oxidant at −78 °C in the presence of xylyl isocyanide.

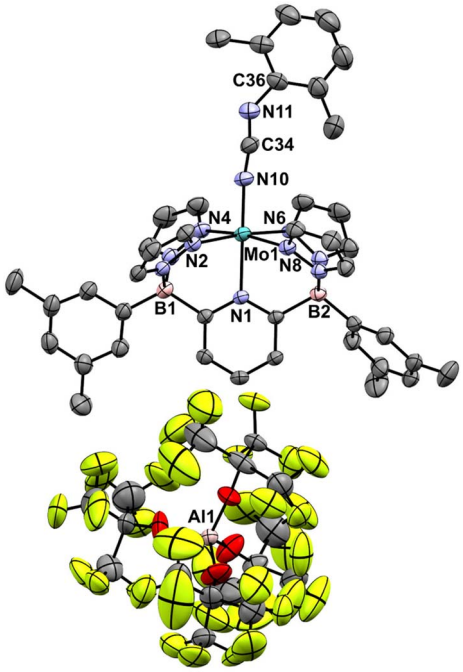

Fig. 6 Molecular structure of **[4-Xyl]**$^+$. Thermal ellipsoids are shown at the 50% probability level and all H atoms are omitted for clarity. Selected bond distances (Å): Mo(1)–N(1), 2.167(3); Mo(1)–N(10), 1.921(3); N(10)–C(34), 1.210(5); C(34)–N(11), 1.207(5); N(11)–C(36), 1.391(6) selected bond angles (°): N(1)–Mo(1)–N(10), 176.82(12); Mo(1)–N(10)–C(34), 171.8(3); N(10)–C(34)–N(11), 170.1(5); C(34)–N(11)–C(36), 137.1(4).

products were observed, consumption of the oxidizing agent was implied by an observed color change to a deep green solution as the solutions slowly warmed. Since we do not observe signals for reduced triarylamine under these conditions, we speculate that the cationic **[1-Ar]**$^+$ products interact with this NAr_3 by-product in some as yet unidentified way. However, if these reactions were carried out in the presence of an isonitrile trapping agent[65] (2,6-dimethylphenylisocyanide), clean conversion to cationic Mo(IV) carbodiimide complexes **[4-Ar]**$^+$ were observed, along with the emergence of signals for NAr_3 (Scheme 6). No reaction was observed between xylyl isocyanide and neutral nitridos **1-Ar**, but upon addition of one equivalent of $[\mathbf{MB}^{\bullet}]^+[Al(OR^F)_4]^-$ at −78 °C, a color change to deep purple was observed as the sample was gradually warmed and production of carbodiimides **[4-Ar]**$^+$ occurred. A separate control experiment showed that xylyl isocyanide is not oxidized by the $[\mathbf{MB}^{\bullet}]^+[Al(OR^F)_4]^-$ oxidant, so we take this as evidence of formation of cations **[1-Ar]**$^+$, which are trapped by the isocyanide reagent to give the observed products.

These Mo(IV) carbodiimide products give assignable proton NMR spectra (Fig. S6†) that clearly indicate incorporation of the xylyl isocyanide reagent. This is also supported by stretching bands (both at 1940 cm^{-1}) in the FTIR spectra of **[4-Tol]**$^+$ and **[4-Xyl]**$^+$, respectively. Dark purple crystals of the latter derivative confirm the structures of these compounds as shown by the molecular structure depicted in Fig. 6. The bond distances and angles (see caption) within the Mo–N=C=N–Xyl unit (particularly the Mo(1)–N(10) distance of 1.921(3) Å and the near linear Mo(1)–N(10)–C(34) angle of 171.8(3)°) are consistent with some double bond character to the Mo(1)–N(10) linkage and C=N double bonds as depicted in Scheme 6.

Conclusions

Nitrogen–nitrogen bond formation *via* coupling of two terminal metal nitrido complexes is one possible pathway for generating N_2 in an ammonia oxidation catalytic scheme. The lowest barrier path for nitrido coupling is to a large degree dictated by the electronic configuration of the L_nMN species (geometry, d electron count, M–N bond order) and the extent to which spin density is or is not localized on the nitrido nitrogen. In the d^1 Mo(V) nitrido complexes **1-Ar** described here, there is very little nitridyl character associated with the MN moiety and so the barrier to N–N bond formation is prohibitively high for this homocoupling path. However, we observe facile loss of N_2 from these compounds upon oxidation with 0.5 equivalents of a one electron oxidant and convincingly demonstrate that this opens up a much lower barrier nucleophilic/electrophilic pathway for N–N bond formation. Oxidation of **1-Ar** to **[1-Ar]**$^+$ flips the nitrido from being nucleophilic in the neutral Mo(V) species to strongly electrophilic in the Mo(VI) cation and induces ambiphilicity into the system, allowing for rapid N–N bond formation.

We believe the "oxidation-induced ambiphilicity" mechanism depicted in Scheme 4 to be a new mechanistic variation

for N–N bond formation from metal nitridos. Some years ago, Che and co-workers observed facile photoinduced N_2 formation from $[(NH_3)_4Os(VI)N]^{3+}$ which was accelerated in the presence of sacrificial electron donors.[66] It was proposed that the N–N bond formation took place by bimolecular coupling between the excited state $[(NH_3)_4Os(VI)N]^{3+}$* and the ground state $[(NH_3)_4Os(VI)N]^{3+}$, which also could be considered a type of "induced ambiphilicity", triggered in this instance by reduction. However, under oxidation catalysis, the path discussed here would likely be more relevant. It is also worth noting that the ECECC path uncovered here is one of several potential N–N bond forming steps in AO catalytic schemes. The favored path (or paths operating in parallel[67]) will be to a large extent dependent on the conditions of the ammonia oxidation catalysis experiments.

The coupling of two metal nitridos to form dinitrogen complexes is the reverse of metal-mediated dinitrogen cleavage,[68] a well-studied reaction of interest in the context of nitrogen fixation to ammonia or other nitrogen containing compounds.[69] While the direction of the reaction is dictated mostly by thermodynamic factors, the kinetics of the preferred process can be significantly influenced by electron configuration and metal geometry. Here, one electron oxidation significantly lowers the barrier of N–N bond formation. In some systems where dinitrogen cleavage is thermodynamically favored, a one electron reduction can lead to significant rate enhancements for metal nitrido formation.[70–72]

Another conclusion from this work re-emphasizes that formation of μ-nitrido bridged dinuclear complexes is a potential pitfall to be considered in the development of catalysts for ammonia oxidation. They can arise in situations where the dominant N–N bond forming step is coupling of two higher valent L_mM^nN compounds. If N_2 release from the μ-dinitrogen product of coupling is more rapid than the N–N coupling step (which is likely on thermodynamic and kinetic grounds) then lower valent L_mM^{n-3} species are formed in the presence of nucleophilic nitrido starting material, leading to the M–N–M products observed here and elsewhere.[4,27,55] Under catalytic conditions, NH_3 would likely effectively compete with $L_mM^{n-3}N$ for the low valent metal centers but ways to avoid formation of μ-nitrido complexes that involved ligand designs aimed at sterically allowing formation of bridging dinitrogen complexes while disfavoring bridging nitrido side products would be worth pursuing.

Data availability

All data related to this article can be found in the ESI document published with this article.†

Author contributions

The manuscript was written through contributions of all authors. CCA and WEP conceived the study and CCA conducted the bulk of the experiments. HDACJ contributed to the Xyl ligand synthesis and Mo starting materials and NR conducted preliminary N_2 elimination experiments for **1-Tol**. LM directed the computational work, which was performed by TR. WZ and BSG contributed some of the X-ray structure determinations. WEP and CCA wrote the manuscript. All authors have given approval to the final version of the manuscript.

Conflicts of interest

There are no conflicts to declare.

Acknowledgements

Funding for this work was provided by NSERC of Canada in the form of a Discovery Grant to W. E. P. who also acknowledges the Canada Research Chair secretariat for a Tier I CRC (2020–2027). C. C. A. thanks Alberta Innovates for scholarship support. The computational work was supported by the HPCs CALcul en Midi-Pyrénées (CALMIP-EOS grant 1415); L. M. is a senior member of the Institut Universitaire de France.

Notes and references

‡ We have found ^{11}B NMR spectral data for the ligand borate moieties to be indicative of the formal oxidation state of the molybdenum centers in these compounds. For example, Mo(III) derivatives fall in the range of −150 to −175 ppm, while the d^1 Mo(V) complexes are generally ^{11}B NMR silent. Mo(IV) complexes, on the other hand, generally resonate in the −40 to −50 ppm range.

1 J. G. Chen, R. M. Crooks, L. C. Seefeldt, K. L. Bren, R. M. Bullock, M. Y. Darensbourg, P. L. Holland, B. Hoffman, M. J. Janik, A. K. Jones, M. G. Kanatzidis, P. King, K. M. Lancaster, S. V. Lymar, P. Pfromm, W. F. Schneider and R. R. Schrock, *Science*, 2018, **360**, eaar6611.
2 M. S. Thompson and T. J. Meyer, *J. Am. Chem. Soc.*, 1981, **103**, 5577–5579.
3 F. Habibzadeh, S. L. Miller, T. W. Hamann and M. R. Smith, *Proc. Natl. Acad. Sci. U. S. A.*, 2019, **116**, 2849–2853.
4 K. Nakajima, H. Toda, K. Sakata and Y. Nishibayashi, *Nat. Chem.*, 2019, **11**, 702–709.
5 P. Bhattacharya, Z. M. Heiden, G. M. Chambers, S. I. Johnson, R. M. Bullock and M. T. Mock, *Angew. Chem., Int. Ed.*, 2019, **58**, 11618–11624.
6 M. D. Zott, P. Garrido-Barros and J. C. Peters, *ACS Catal.*, 2019, **9**, 10101–10108.
7 Y. Li, J.-Y. Chen, Q. Miao, X. Yu, L. Feng, R.-Z. Liao, S. Ye, C.-H. Tung and W. Wang, *J. Am. Chem. Soc.*, 2022, **144**, 4365–4375.
8 P. L. Dunn, B. J. Cook, S. I. Johnson, A. M. Appel and R. M. Bullock, *J. Am. Chem. Soc.*, 2020, **142**, 17845–17858.
9 V. Smil, *Enriching the Earth: Fritz Haber, Carl Bosch, and the Transformation of World Food Production*, MIT Press, Cambridge, MA, 2001.
10 M. J. Bezdek, S. Guo and P. J. Chirik, *Science*, 2016, **354**, 730.
11 M. J. Bezdek, I. Pelczer and P. J. Chirik, *Organometallics*, 2020, **39**, 3050–3059.
12 P. Bhattacharya, Z. M. Heiden, E. S. Wiedner, S. Raugei, N. A. Piro, W. S. Kassel, R. M. Bullock and M. T. Mock, *J. Am. Chem. Soc.*, 2017, **139**, 2916–2919.

13 B. J. Cook, M. Barona, S. I. Johnson, S. Raugei and R. M. Bullock, *Inorg. Chem.*, 2022, **61**, 11165–11172.
14 S. I. Johnson, S. P. Heins, C. M. Klug, E. S. Wiedner, R. M. Bullock and S. Raugei, *Chem. Commun.*, 2019, **55**, 5083–5086.
15 C. C. Almquist, N. Removski, T. Rajeshkumar, B. S. Gelfand, L. Maron and W. E. Piers, *Angew. Chem., Int. Ed.*, 2022, **61**, e202203576.
16 J. J. Warren, T. A. Tronic and J. M. Mayer, *Chem. Rev.*, 2010, **110**, 6961–7001.
17 R. G. Agarwal, S. C. Coste, B. D. Groff, A. M. Heuer, H. Noh, G. A. Parada, C. F. Wise, E. M. Nichols, J. J. Warren and J. M. Mayer, *Chem. Rev.*, 2022, **122**, 1–49.
18 H. Toda, K. Kuroki, R. Kanega, S. Kuriyama, K. Nakajima, Y. Himeda, K. Sakata and Y. Nishibayashi, *ChemPlusChem*, 2021, **86**, 1511–1516.
19 M. J. Trenerry, C. M. Wallen, T. R. Brown, S. V. Park and J. F. Berry, *Nat. Chem.*, 2021, **13**, 1221–1227.
20 N. X. Gu, P. H. Oyala and J. C. Peters, *Angew. Chem., Int. Ed.*, 2021, **60**, 4009–4013.
21 M. E. Ahmed, M. Raghibi Boroujeni, P. Ghosh, C. Greene, S. Kundu, J. A. Bertke and T. H. Warren, *J. Am. Chem. Soc.*, 2022, **146**, 21136–21145.
22 S.-M. Yiu, W. W. Y. Lam, C.-M. Ho and T.-C. Lau, *J. Am. Chem. Soc.*, 2007, **129**, 803–809.
23 M. G. Scheibel, B. Askevold, F. W. Heinemann, E. J. Reijerse, B. de Bruin and S. Schneider, *Nat. Chem.*, 2012, **4**, 552–558.
24 M. G. Scheibel, J. Abbenseth, M. Kinauer, F. W. Heinemann, C. Würtele, B. de Bruin and S. Schneider, *Inorg. Chem.*, 2015, **54**, 9290–9302.
25 T. Miyazaki, H. Tanaka, Y. Tanabe, M. Yuki, K. Nakajima, K. Yoshizawa and Y. Nishibayashi, *Angew. Chem., Int. Ed.*, 2014, **53**, 11488–11492.
26 D. C. Ware and H. Taube, *Inorg. Chem.*, 1991, **30**, 4605–4610.
27 S. B. Seymore and S. N. Brown, *Inorg. Chem.*, 2002, **41**, 462–469.
28 S. V. Park, A. R. Corcos, A. N. Jambor, T. Yang and J. F. Berry, *J. Am. Chem. Soc.*, 2022, **144**, 3259–3268.
29 M. E. de Vries, R. M. La Crois, G. Roelfes, H. Kooijman, A. L. Spek, R. Hage and B. L. Feringa, *Chem. Commun.*, 1997, 1549–1550, DOI: **10.1039/A702804K**.
30 R. T. Jonas and T. D. P. Stack, *J. Am. Chem. Soc.*, 1997, **119**, 8566–8567.
31 R. J. M. Klein Gebbink, R. T. Jonas, C. R. Goldsmith and T. D. P. Stack, *Inorg. Chem.*, 2002, **41**, 4633–4641.
32 H. I. Karunadasa, C. J. Chang and J. R. Long, *Nature*, 2010, **464**, 1329–1333.
33 Y. Sun, J. P. Bigi, N. A. Piro, M. L. Tang, J. R. Long and C. J. Chang, *J. Am. Chem. Soc.*, 2011, **133**, 9212–9215.
34 V. S. Thoi, Y. Sun, J. R. Long and C. J. Chang, *Chem. Soc. Rev.*, 2013, **42**, 2388–2400.
35 D. Z. Zee, T. Chantarojsiri, J. R. Long and C. J. Chang, *Acc. Chem. Res.*, 2015, **48**, 2027–2036.
36 D. M. Spasyuk, S. H. Carpenter, C. E. Kefalidis, W. E. Piers, M. L. Neidig and L. Maron, *Chem. Sci.*, 2016, **7**, 5939–5944.
37 D. W. Beh, W. E. Piers, I. del Rosal, L. Maron, B. S. Gelfand, C. Gendy and J. B. Lin, *Dalton Trans.*, 2018, **47**, 13680–13688.
38 D. W. Beh, W. E. Piers, B. S. Gelfand and J.-B. Lin, *Dalton Trans.*, 2020, **49**, 95–101.
39 D. W. Beh, W. E. Piers, L. Maron, Y. Yang, B. S. Gelfand and J.-B. Li, *Polyhedron*, 2020, **179**, 114410.
40 L. Nurdin, D. M. Spasyuk, L. Fairburn, W. E. Piers and L. Maron, *J. Am. Chem. Soc.*, 2018, **140**, 16094–16105.
41 L. Nurdin, D. M. Spasyuk, W. E. Piers and L. Maron, *Inorg. Chem.*, 2017, **56**, 4157–4168.
42 L. Nurdin, Y. Yang, P. G. N. Neate, W. E. Piers, L. Maron, M. L. Neidig, J. B. Lin and B. S. Gelfand, *Chem. Sci.*, 2021, **12**, 2231–2241.
43 D. W. Beh, A. J. Cuellar De Lucio, I. del Rosal, L. Maron, D. Spasyuk, B. S. Gelfand, J.-B. Li and W. E. Piers, *Organometallics*, 2023, **42**, 1149–1157.
44 D. F. Evans, *J. Chem. Soc.*, 1959, 2003–2005, DOI: **10.1039/JR9590002003**.
45 J. C. Kim, W. S. Rees Jr and V. L. Goedken, *Inorg. Chem.*, 1995, **34**, 2483–2486.
46 P. Basu, *J. Chem. Educ.*, 2001, **78**, 666.
47 S. Verma and M. Hanack, *Z. Anorg. Allg. Chem.*, 2003, **629**, 880–892.
48 E. Seikel, B. Oelkers, O. Burghaus and J. Sundermeyer, *Inorg. Chem.*, 2013, **52**, 4451–4457.
49 I. Krossing, *Chem.–Eur. J.*, 2001, **7**, 490–502.
50 N. G. Connelly and W. E. Geiger, *Chem. Rev.*, 1996, **96**, 877–910.
51 M. R. Talipov, M. M. Hossain, A. Boddeda, K. Thakur and R. Rathore, *Org. Biomol. Chem.*, 2016, **14**, 2961–2968.
52 I. M. Riddlestone, A. Kraft, J. Schaefer and I. Krossing, *Angew. Chem., Int. Ed.*, 2018, **57**, 13982–14024.
53 P. L. Dunn, S. I. Johnson, W. Kaminsky and R. M. Bullock, *J. Am. Chem. Soc.*, 2020, **142**, 3361–3365.
54 R. M. Clarke and T. Storr, *J. Am. Chem. Soc.*, 2016, **138**, 15299–15302.
55 M. Keener, M. Peterson, R. Hernández Sánchez, V. F. Oswald, G. Wu and G. Ménard, *Chem.–Eur. J.*, 2017, **23**, 11479–11484.
56 T. Chantarojsiri, A. H. Reath and J. Y. Yang, *Angew. Chem., Int. Ed.*, 2018, **57**, 14037–14042.
57 J. Du Bois, C. S. Tomooka, J. Hong and E. M. Carreira, *Acc. Chem. Res.*, 1997, **30**, 364–372.
58 C. E. Laplaza, M. J. A. Johnson, J. C. Peters, A. L. Odom, E. Kim, C. C. Cummins, G. N. George and I. J. Pickering, *J. Am. Chem. Soc.*, 1996, **118**, 8623–8638.
59 C. Schiller, D. Sieh, N. Lindenmaier, M. Stephan, N. Junker, E. Reijerse, A. A. Granovsky and P. Burger, *J. Am. Chem. Soc.*, 2023, **145**, 11392–11401.
60 G. P. Connor, B. Q. Mercado, H. M. C. Lant, J. M. Mayer and P. L. Holland, *Inorg. Chem.*, 2019, **58**, 10791–10801.
61 D. Martelino, S. Mahato, W. VandeVen, N. M. Hein, R. M. Clarke, G. A. MacNeil, F. Thomas and T. Storr, *J. Am. Chem. Soc.*, 2022, **144**, 11594–11607.
62 E. D. Hedegård, J. Bendix and S. P. A. Sauer, *J. Mol. Struct.: THEOCHEM*, 2009, **913**, 1–7.
63 F. Hasanayn, P. L. Holland, A. S. Goldman and A. J. M. Miller, *J. Am. Chem. Soc.*, 2023, **145**, 4326–4342.

64 L. S. Yamout, M. Ataya, F. Hasanayn, P. L. Holland, A. J. M. Miller and A. S. Goldman, *J. Am. Chem. Soc.*, 2021, **143**, 9744–9757.
65 A. K. Maity, J. Murillo, A. J. Metta-Magaña, B. Pinter and S. Fortier, *J. Am. Chem. Soc.*, 2017, **139**, 15691–15700.
66 H.-W. Lam, C.-M. Che and K.-Y. Wong, *J. Chem. Soc., Dalton Trans.*, 1992, 1411–1416, DOI: **10.1039/DT9920001411**.
67 C.-P. Chen, W. Alharbi, T. R. Cundari, T. W. Hamann and M. R. Smith III, *J. Am. Chem. Soc.*, 2023, **145**, 26339–26349.
68 S. J. K. Forrest, B. Schluschaß, E. Y. Yuzik-Klimova and S. Schneider, *Chem. Rev.*, 2021, **121**, 6522–6587.
69 S. Kuriyama and Y. Nishibayashi, *Tetrahedron*, 2021, **83**, 131986.
70 J. C. Peters, J.-P. F. Cherry, J. C. Thomas, L. Baraldo, D. J. Mindiola, W. M. Davis and C. C. Cummins, *J. Am. Chem. Soc.*, 1999, **121**, 10053–10067.
71 D.-D. Zhai, S.-Q. Zhang, S.-J. Xie, R.-K. Wu, F. Liu, Z.-F. Xi, X. Hong and Z.-J. Shi, *J. Am. Chem. Soc.*, 2022, **144**, 14071–14078.
72 G. P. Connor, D. Delony, J. E. Weber, B. Q. Mercado, J. B. Curley, S. Schneider, J. M. Mayer and P. L. Holland, *Chem. Sci.*, 2022, **13**, 4010–4018.